

Validation of the strike point position estimation with the local expansion method for MAST Upgrade on the DIII-D tokamak

H. Anand¹, D. Eldon¹, M. Kochan², G. McArdle², L. Pangione²,
and H.Q. Wang¹

¹*DIII-D National Fusion Facility, General Atomics, PO Box 85608, San Diego, CA
92186, USA*

²*Culham Centre for Fusion Energy, Culham Science Centre, Abingdon, OX14 3DB,
United Kingdom*

Abstract

A local expansion method has been proposed for estimating the strike point position for the advanced divertor configuration on the MAST Upgrade tokamak. The paper discusses the application and assesses the performance of the technique on a long-legged divertor plasma configuration on an operating device - the DIII-D tokamak. A comparison of the spatial location of the outer strike point estimated with the local expansion method against the plasma boundary reconstruction and divertor diagnostics on the DIII-D tokamak is reported. A good agreement with the equilibrium reconstruction and diagnostic data is achieved with respect to estimation of the spatial location of the outer strike point for the long-legged divertor plasma discharge.

Keywords— plasma control, local flux expansion, strike point, divertor, reconstruction, real-time

1 Introduction

The MAST Upgrade (MAST-U) tokamak [1] will explore extended- and expanded-leg divertor geometries, including the Super-X plasma configuration [2] (shown in Figure 1), while allowing higher-performance core-plasma operations without excessive erosion and/or damage to the divertor target. Accurate real-time (RT) determination of the novel divertor magnetic field configuration, including spatial location of the divertor leg extension, will be required as an input to some proposed control systems. For example, a detachment control system using

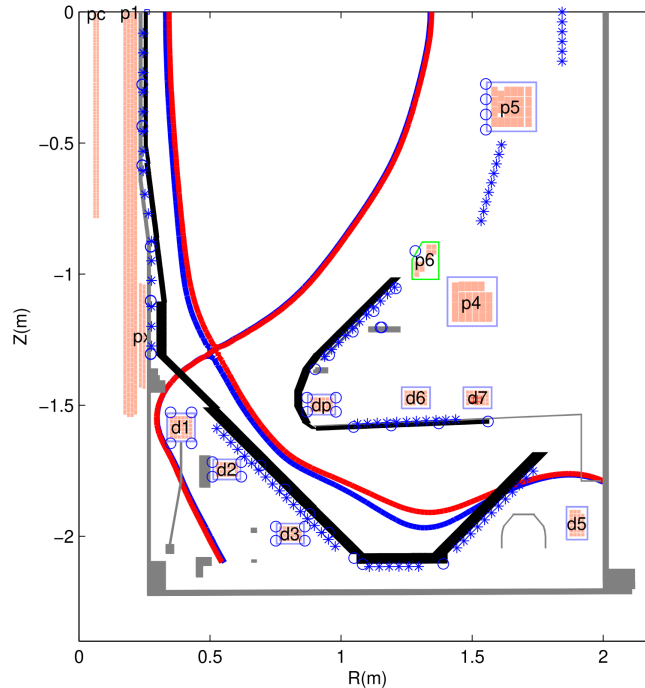


Figure 1: An example super-X divertor configuration in MAST-U. The magnetic probes are shown as blue crosses and flux loops as the circles. Coils are as labelled, vessel structure is grey. A hypothetical best estimate for the true separatrix position is given by the red curve, compared to a hypothetical result from local expansion approach in blue, with some error between them.

Langmuir probes [3] would need to know which probe(s) to read depending on the strike point position at any given time. Several approaches to RT tokamak equilibrium reconstruction have been developed and are in routine use on operating devices [4, 5, 6]. They involve identifying, from experimental measurements, a distribution of the plasma current density that satisfies the pressure balance constraint and provide an accurate determination of the plasma shape (plasma position, triangularity, elongation, gaps between the plasma surface and vessel wall etc.) and the divertor parameters (X-point position, inner and outer strike point positions etc.). However, as shown in Figure 1, with long-legged exotic divertor configuration, such as MAST-U, the application of equilibrium reconstruction alone for strike point estimation may be inaccurate. The inaccuracy can arise particularly in the case of high-order divertor x-point configurations and long divertor legs. Both of these configurations are relatively weakly constrained by the core equilibrium and boundary characteristics themselves, and thus can benefit from additional constraints more local to the divertor. In the case of MAST-U, due to the larger area of the divertor region in comparison to the present tokamaks, the experimental measurements used as inputs to the equilibrium reconstruction are obtained far from the plasma surface in the divertor region and the equilibrium solution is largely governed by the measurements

surrounding the core plasma. Along with the vacuum vessel itself, MAST-U hosts significant number of in-vessel structures, including the passive stabilization plates [7]. Located between the confined plasma and the strike points, these augment the vertical stabilization, and the effect of transient currents in the structures due to the plasma motion will impact the magnetic measurement in the nearby vicinity which can have an impact on the estimation of the outer strike point position from the equilibrium reconstruction method. A local higher order expansion of poloidal flux calculations constrained by the vacuum field equation, fitted to the magnetic field and flux measurements in the nearby vicinity of the divertor leg can provide an accurate RT estimation of the outer strike point on MAST-U tokamak. Such techniques have already been used successfully for plasma boundary reconstruction on the JET and EAST tokamak [8, 9]. Thus, the local poloidal flux expansion method promises to be a strong candidate for providing fast and reliable estimation of outer strike point for the advanced divertor configuration on the MAST-U tokamak.

This paper describes the implementation and benchmarking of the local poloidal flux expansion method developed for MAST-U on the DIII-D tokamak. Section 2 introduces the DIII-D tokamak, experimental setup and the existing off-line and RT equilibrium reconstruction methods. Section 3 shows a good comparison of the outer strike position from the off-line equilibrium reconstruction and the Langmuir probe (LP) diagnostic data for a long-legged DIII-D divertor plasma discharge and justifies the choice of using the off-line equilibrium reconstruction as a reference for comparing the local expansion method and RT equilibrium reconstruction. Section 4 introduces the fundamental concepts of the local expansion method and its implementation on a long-legged DIII-D divertor plasma discharge type, along with the comparison against RT equilibrium reconstruction. A brief overview of the method, implementation and results, as well as an outlook for the physics applications of the local poloidal flux expansion method to advanced divertor plasma configurations is provided in Section 5.

2 DIII-D tokamak and experimental setup

The main operational parameters of the DIII-D tokamak are the following: typical major radius 1.69 m, typical minor radius 0.60 m, vacuum toroidal field up to 2.2 T, plasma current up to 2 MA, elongation up to 2.0 [10]. DIII-D also hosts a flexible poloidal-field coil system that allows tests with long-legged divertors. The magnetic diagnostic system of the DIII-D tokamak includes approximately 250 inductive sensors of various types, including axisymmetric poloidal flux loops and pickup coils [11]. The extensive set of magnetic sensors, extreme shaping versatility and the presence of the Grad-Shafranov equilibrium reconstruction code, EFIT [12] and its RT version, RTEFIT [4] sets a strong foundation for benchmarking the local expansion algorithm for strike point location estimation developed for MAST-U and tested on the DIII-D tokamak.

On the DIII-D tokamak, plasma discharge parameters are evaluated from fitting the diagnostic data to the Grad-Shafranov model, which describes the force balance of the tokamak equilibrium, while allowing for a distributed current source. This full reconstruction of the equilibrium that is performed off-line using a computationally intensive fitting algorithm is referred to as EFIT [13]. However, to compute discharge parameters in real-time for feedback control, a RT solution to the Grad-Shafranov equation is calculated in a way that provides a close approximation to the solution over short timescales (< 1 ms), and converges to an increasingly accurate solution over longer timescales ($>$ a few ms). The solutions are produced at a rate sufficient for plasma discharge control and this equilibrium reconstruction algorithm is referred to as RTEFIT [4]. Small differences in various plasma discharge parameters between EFIT and RTEFIT are expected and the reasons are discussed in [4]. Furthermore, for the work presented in the paper, we will refer to the set of results from EFIT01 and EFITRT1, respectively. EFIT01 refers to a set of EFIT calculations which are run automatically after each DIII-D shot using simple (e.g. MSE data are not used) but consistent settings. EFITRT1 is the set of RT reconstructions which are used for plasma shape control and thus is widely available. Other sets of EFIT results are published under different labels, such as EFIT02 for results using motional Stark effect (MSE).

Figure 2(a) shows a series of magnetic equilibria for a L-mode plasma discharge, #147740 from EFIT01. The main plasma parameters are as follows: plasma current, $I_p = 0.8$ MA, injected power, $P_{INJ} = 1.2$ MW and line-averaged density normalized to the Greenwald density, $n_e/n_G = 0.2$. The plasma discharge involves a variation in the radial placement of the outer divertor strike point, R_{OSP} , ranging from 1.20 m to 1.61 m as shown in (Figure 2(b)). The evolution of the R_{OSP} and poloidal flux at the X-point, ψ_X from EFIT01 and EFITRT1 is shown in Figure 2(b,c). As expected, small differences in the plasma discharge parameters are observed between the two equilibrium reconstruction methods. All the comparison and validation results presented in future sections will use the plasma discharge, #147740 as the reference plasma configuration.

3 Comparison of R_{OSP} from EFIT and LPs

The position of the strike point can be verified using profiles from Langmuir probe [15] measurements, as the probes are fixed to the plasma facing surfaces at known locations (the locations are shown in Figure 2(d)). The external voltage applied to each probe is swept, and the changes in current collected by the probe tip is measured. Analysis of the so-called I/V characteristic directly yields electron temperature T_e , ion saturation current density J_{sat} , and floating potential ϕ_f [15, 16]; from these, electron density n_e and parallel heat flux (not including ionization potential) $q_{||}$ can be derived.

These profiles are most accurately measured during strike point sweeps, where

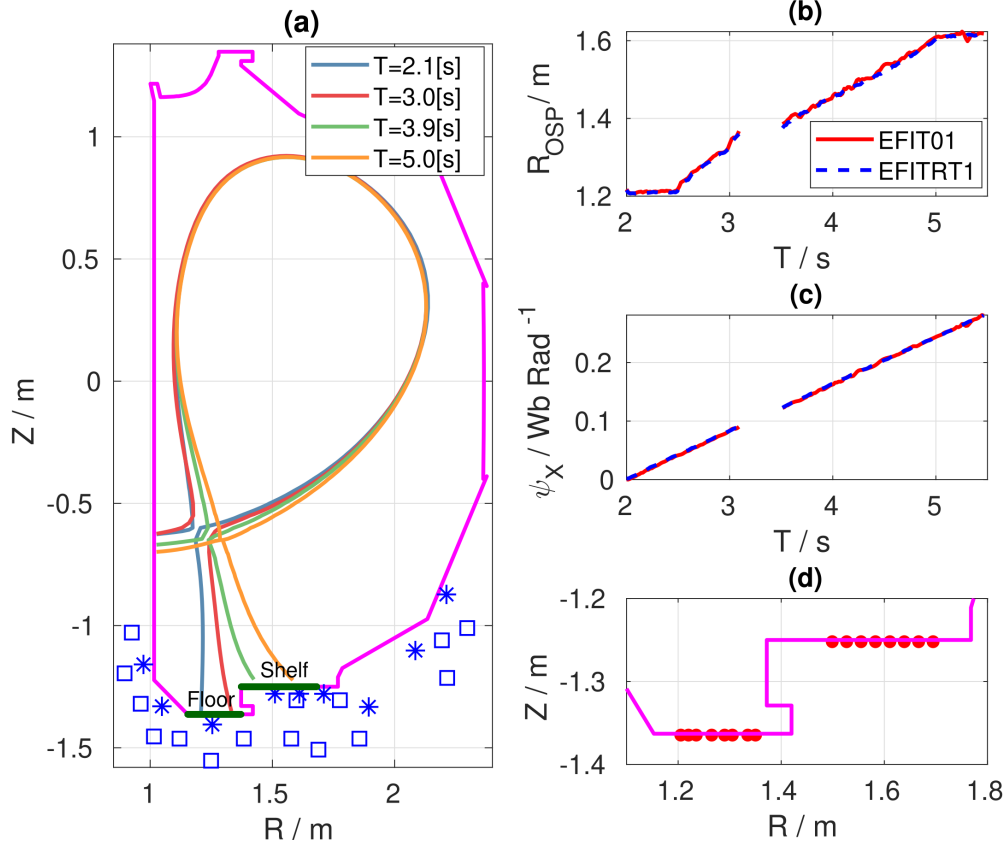


Figure 2: (a) Plasma magnetic equilibria from EFIT01 for #147740 at various time instants. The blue squares and stars give the position of the flux loops and pickup coils and the solid dark green line denotes the part of the divertor contour used by local poloidal flux expansion method. Time evolution of: (b) radial position of the outer strike point, R_{OSP} and (c) poloidal flux at the separatrix, ψ_X from EFIT01 and EFITRT1. (d) Zoomed view of the divertor region with the Langmuir probe arrays shown as red filled circles. The empty region between the time interval 3.1 s - 3.5 s denotes the transition of the plasma equilibrium from the floor to the divertor shelf and is not accounted for the analysis.

the motion of the strike point (Figure 2(b)) fills in the profile. Referring to the floor and shelf regions marked in Figure 2, Langmuir probe arrays cover the ranges $1.207 \leq R \leq 1.352$ m on the floor and $1.500 \leq R \leq 1.696$ m on the shelf, where R is the radial coordinate. The relevant time ranges for obtaining good probe measurements during the strike point sweep in shot 147740 should be $2.5 < t < 3.1$ and $4.2 < t < 5$ s. These time-ranges can be subdivided into smaller intervals, each long enough for the strike point to move from one probe to the next, to measure different systematic errors in EFIT01's strike point position when the strike point is near different magnetic probes. The end goal is to obtain a time-varying correction (which can be interpolated between the analysis windows) that can be added to EFIT01's nominal result to cancel out

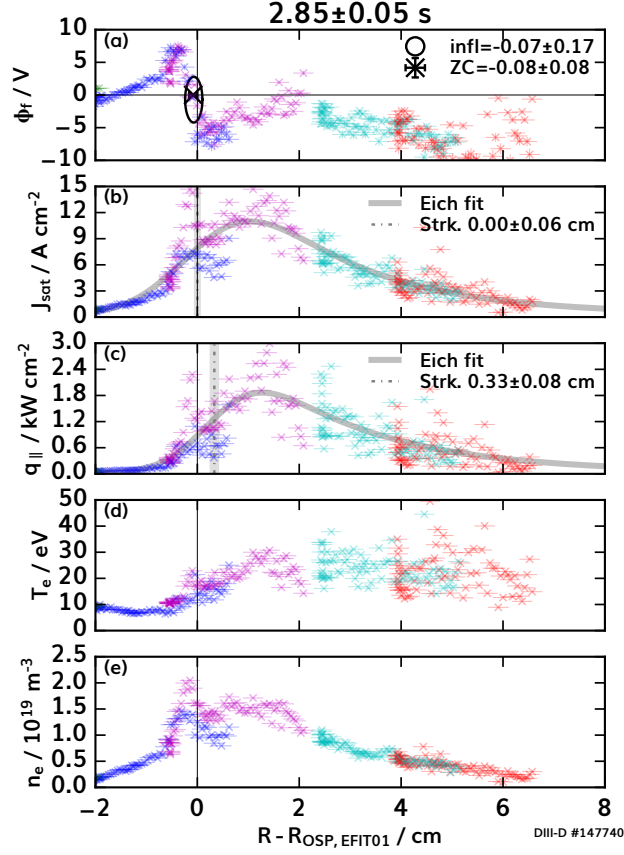


Figure 3: Profiles of LP measurements, plotted relative to EFIT01’s strike point position, used to estimate a correction to EFIT01’s strike point position. Colors correspond to different physical probes. Error bars on the individual samples (“x”s) represent the probe tip size. The ϕ_f profile (a) has an X (with error bars) marking the estimated zero-crossing point, and an ellipse marking the estimated inflection point location. The J_{sat} (b) and $q_{||}$ (c) plots are overlaid with a dash-dotted black line and gray band representing the strike point position given by Eich’s function [14], with the function itself shown with gray curves. T_e (d) and n_e (e) are provided for reference.

its systematic error.

Figure 3 shows profiles of several probe measurements during a sample time window plotted against $R - R_{OSP, EFIT01}$, where R is the measured position of the Langmuir probe and $R_{OSP, EFIT01}$ is the radial position of the outer strike point estimated by EFIT01; the strike point should be at 0 if EFIT01 is performing perfectly. We can estimate the actual position of the strike point position from landmarks in the floating potential ϕ_f profile and from Eich fits [14] to heat flux $q_{||}$ and ion saturation current density J_{sat} profiles; strike point position is a fit parameter in Eich’s function. The Eich fit is designed for heat flux, but the shape is empirically similar to the J_{sat} profile and the arguments behind its

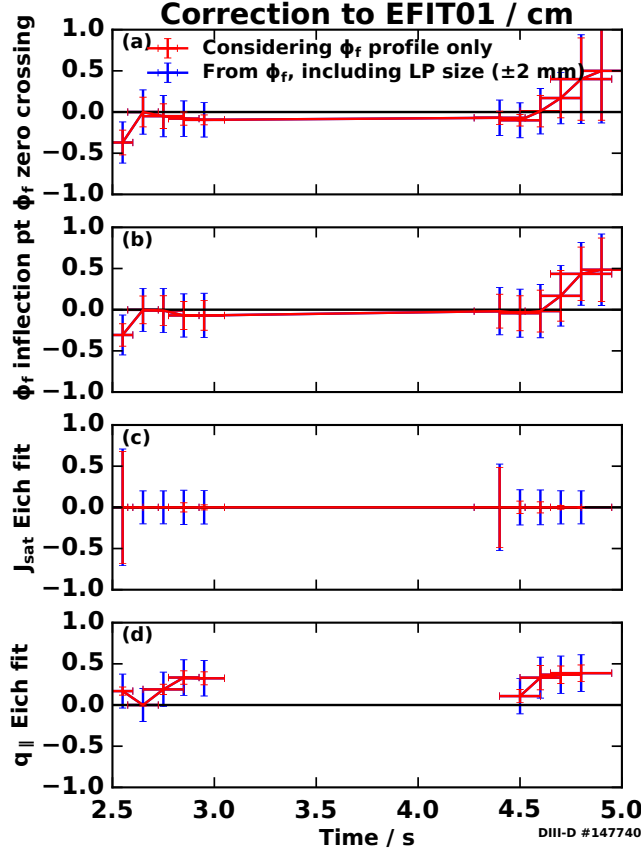


Figure 4: Corrections to EFIT01 vs. time, using various methods: the manually estimated zero-crossing of Langmuir probe ϕ_f profiles to define the true strike point position (a), manually estimated inflection point of the ϕ_f profile (b), strike point position extracted from Eich [14] fits to J_{sat} (c), and strike point position from Eich fits to heat flux (d). The LPs have 4 mm wide tips [15], so 2 mm error has been added in quadrature with other errors.

terms seem sensible, so it serves as a basis for strike point position estimation. The ϕ_f profile should have an inflection point at the separatrix [17]. This is typically located very close to a zero-crossing, and zero-crossings are easier to locate in noisy data. The locations of both landmarks for each ϕ_f profile have been estimated by manual inspection, with uncertainty in position based on scatter in the data (approximately the width of the band of scattered data for zero-crossings). Although we have not used methods of estimating strike point position using T_e and n_e directly, they factor into heat flux and may be of some interest and thus are included in Figure 3. Note that the high density in the private flux region (PFR) in Figure 3(e) could be due to an $E_\theta \times B$ drift flow pushing particles from the scrape-off layer (SOL) to PFR.

Figure 4 shows the corrections from several profiles taken from different time windows; each is similar to the sample shown in figure 3. The direct uncertainty

(red) from the estimates can be increased (blue) to account for the 2 mm half-width of the probe tips [15]. With this in mind, the ϕ_f zero-crossing and inflection point methods provide essentially no correction, and neither does the Eich fit to J_{sat} . The fits to q_{\parallel} suggest a correction of up to 3.9 ± 1.0 mm, but the average correction from the slices considered is 2.5 ± 0.3 mm. The average corrections indicated by the ϕ_f zero-crossing, ϕ_f inflection point, and J_{sat} Eich fit methods are 0.3 ± 0.8 , 0.5 ± 0.7 , and 0 ± 0.8 mm. The ϕ_f methods suggest an increasing correction with time, but the uncertainty also increases. Taken together, these results do not confidently suggest a meaningful correction to EFIT01 for this shot and its reported strike point position should be taken as the best estimate for the true strike point position, with an uncertainty of about 4 mm. That is, we can neglect systematic errors in the strike point position reported by EFIT01 for this DIII-D shot. This is consistent with past experience: EFIT01 typically agrees well with the Langmuir probes in the lower half of the machine [18]. It is also typical for EFITRT1 and EFIT01 to disagree by ≈ 1 cm [18].

4 The local poloidal flux expansion method

The local poloidal flux expansion method utilizes 6^{th} order expansions of the poloidal flux function, constrained by the vacuum field equations. The formulation of the expansion is given as follows [8]:

$$\psi(R, Z) = \sum_{\substack{i=0 \\ j=0 \\ i+j \leq 6}}^6 a_{ij} \rho^i z^j \quad (1)$$

where, $\rho = R^2 - R_0^2$, $z = Z - Z_0$ and (R_0, Z_0) is the center point of expansion.

The coefficients of expansion, a_{ij} are determined by imposing the vacuum magnetic field equation (2) and by fitting to the local poloidal flux values from the flux loops and magnetic field measurements from the pickup coils.

$$\Delta^* \psi = 0; \Delta^* = \partial_{RR} + \partial_{ZZ} - \frac{1}{R} \partial_R \quad (2)$$

The 6^{th} -order local expansion leads to 8 independent coefficients to be determined. The detailed derivation with respect to the number of coefficients for a given order is reported in the appendix [9]. The performance of the local expansion method with various order's of expansion and the justification for using the 6^{th} -order local expansion is discussed later in the text. The poloidal flux and the magnetic field can be written in terms of these coefficients as follows:

$$\begin{aligned}\psi_e(\rho, z) &= \sum_{i=1}^{13} \psi_i(\rho, z) C_i \\ B_e(\rho, z) &= \sum_{i=1}^{13} B_i(\rho, z) C_i\end{aligned}\tag{3}$$

where, ψ_e and B_e are the estimated values of the flux and magnetic field for a sensor with index j at (R_j, Z_j) . The coefficients, C_i are obtained by minimizing equation:

$$\chi^2 = \frac{1}{2} \sum_{Flux\ loops} (\psi_m(j) - \psi_e(j))^2 + \frac{1}{2} \sum_{Pickup\ coils} (B_m(j) - B_e(j))^2\tag{4}$$

where, ψ_m and B_m are the measured values of the flux and magnetic field at R_j, Z_j . The Equation (4) can further be simplified in the following form:

$$\chi^2 = \frac{1}{2} \sum_{j=1}^{N_m} \left(m_j - \sum_{i=1}^{13} d_{ji} C_i \right)^2\tag{5}$$

where, $m_j \equiv \psi_m, B_m$ are the measurements, $d_{ji} \equiv \psi_i(\rho_j, z_j), B_i(\rho_j, z_j)$ and N_m is the number of measurements. The minimization can be summarized as:

$$D\vec{C} = \vec{M}\tag{6}$$

where, $D_{ki} = \sum_{j=1}^{N_m} d_{ji} d_{jk}$ and $M_k = \sum_{j=1}^{N_m} d_{jk} m_j$, respectively. In the presence of active coils inside the vacuum region, the local expansion method requires measurements from which the contributions of the coils have been removed. These contributions are then added back to the flux reconstruction later. Since the local expansion method is used for slow control of the plasma boundary and not applied to fast transitions (few ms, 0.5 ms - 10 ms for DIII-D), the effect of the eddy currents induced in the passive structures can be neglected. Complete details about the method, along with the fully analytic form of the poloidal flux expansion can be found in [8, 9].

The local expansion method was applied to the DIII-D plasma discharge shown in Figure 2(a) for the determination of poloidal flux on the part of the 2-D divertor contour, representing the floor and the shelf (Figure 2(a)). The location of the flux loops and pickup coils used in the local expansion method are also shown in Figure 2(a). Using the geometrical description of flux loops and pickup coils, D was constructed and the expansion coefficients, \vec{C} were determined during the plasma evolution with the help of Equation (6) for each set of \vec{M} . Using the geometrical description of the 2-D divertor contour and with information on the expansion coefficient, poloidal flux on the floor and shelf was estimated for each time instant using the local expansion method.

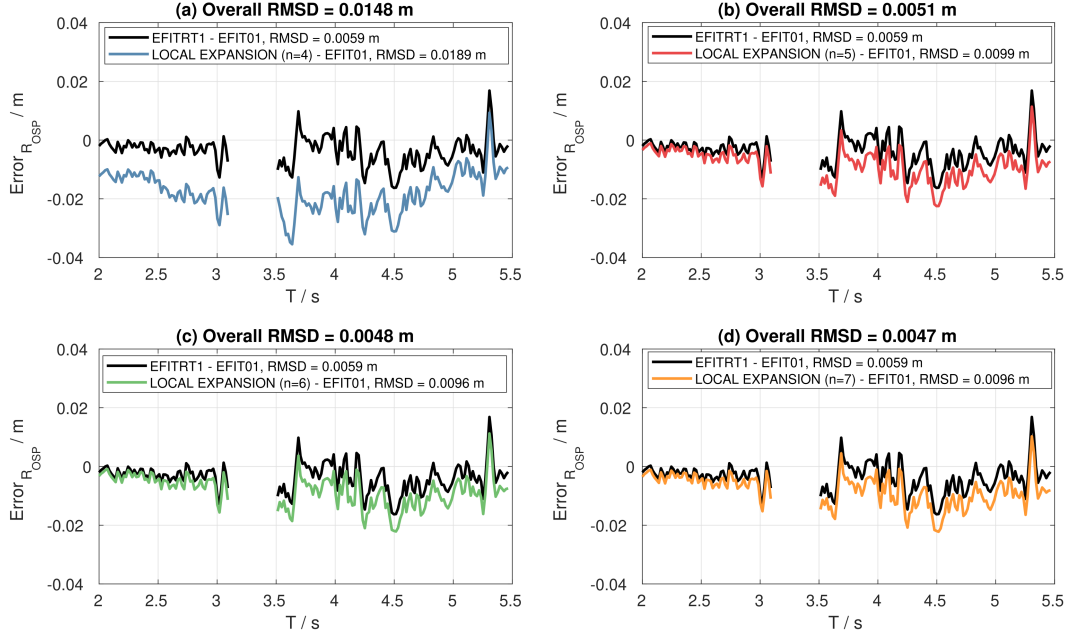


Figure 5: (a-d) Evolution of the error in R_{OSP} between EFIT01 and EFITRT1 Vs. EFIT01 and local expansion for different order of polynomial expansion. The empty region between the time interval 3.1 s - 3.5 s denotes the transition of the plasma equilibrium from the floor to the divertor shelf and is not accounted for the analysis.

Generally, the estimation of R_{OSP} requires the prior knowledge of ψ_X and corresponds to the spatial location on the 2-D divertor contour at which the poloidal flux value matches with ψ_X . In principle, similar to the estimation of poloidal flux on the 2-D divertor contour, the local expansion method can also be applied for the determination of ψ_X with the help of the magnetic sensors in the nearby vicinity. However for the sake of a fair comparison, ψ_X from EFITRT1 is used for the determination of R_{OSP} in both, the local expansion method and EFITRT1 itself.

Due to the excellent agreement with the LP diagnostic data as shown in Section 3, EFIT01 is used as the nominal reference. Figure 5(a-d) shows the difference in the performance of the local expansion method for various orders of polynomial expansion. The performance for each order of polynomial expansion is determined by evaluating the root mean square deviation (RMSD) between the error in R_{OSP} between EFITRT1 and EFIT01, and the error in the local expansion method and EFIT01, respectively. The associated overall RMSD values for each order is listed in the title of the subplots in Figure 5(a-d). Also, note that the RMSD in R_{OSP} between local expansion method with different orders and EFIT01, along with the RMSD between EFITRT1 and EFIT01 are listed inside the legend of the subplots of Figure 5(a-d). For the DIII-D plasma

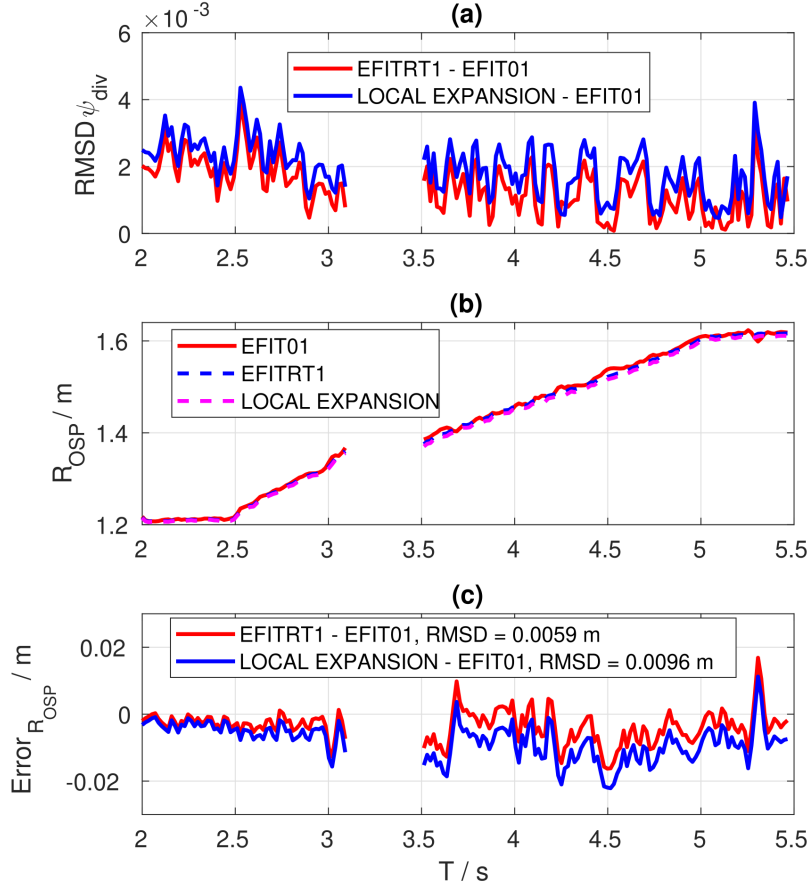


Figure 6: (a) Evolution of the RMSD of ψ_{div} between EFIT01 and EFITRT1 Vs. EFIT01 and the local expansion method with 5^{th} order polynomial expansion. (b) Evolution of R_{OSP} from EFIT01, EFITRT1 and local expansion with 5^{th} order polynomial expansion. (c) Evolution of the error in R_{OSP} between EFIT01 and EFITRT1 Vs. EFIT01 and local expansion with 5^{th} order polynomial expansion. The empty region between the time interval 3.1 s - 3.5 s denotes the transition of the plasma equilibrium from the floor to the divertor shelf and is not accounted for the analysis.

discharge shown in Figure 2(a), a comparable performance of the local flux expansion method is obtained with a 5^{th} , 6^{th} and 7^{th} order polynomial, with the RMSD value of ≈ 0.005 m between the error in R_{OSP} between EFITRT1 and EFIT01, and the error in the local expansion method and EFIT01. Obviously, the results of 4^{th} order are not acceptable due to higher RMSD values in comparison to higher order polynomials. In general, a lower order expansion might discard poloidal flux distribution information in the vacuum region, especially for plasma configuration with higher order moments of the magnetic distribution, reducing the reconstruction accuracy. On the other hand, the maximum order

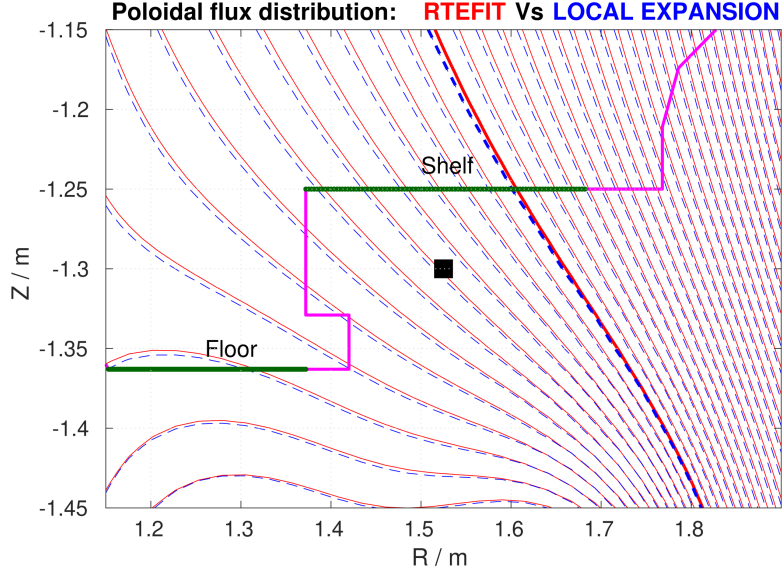


Figure 7: Comparison of the poloidal flux distribution for the plasma discharge shown in Figure 2(a) reconstructed by the local expansion method with 6th order polynomial expansion and EFITRT1. The reconstructed separatrix and isoflux contours from the local expansion method is shown by the blue solid and dashed line. It is superimposed on the EFITRT1 separatrix and isoflux contours denoted by the red solid and dashed line. The solid black square denotes the centre point of the expansion. The position of the flux loops and pickup coils used by the local flux expansion method is shown in Figure 2(a).

of the expansion is limited by the availability and distribution of magnetic sensor. In addition, a higher order polynomial expansion may results in artifacts in reconstruction. The optimum expansion order is a trade-off of the above factors and thus a 6th order polynomial is sufficient for the study presented in the paper.

With 6th order polynomial expansion, the difference in the performance with respect to EFITRT1 is found by comparing the estimation of the poloidal flux on the floor and shelf, comprising the 2-D divertor contour, ψ_{div} and R_{OSP} relative to EFIT01 values, as shown in Figure 6. ψ_{div} with EFITRT1 and EFIT01 is directly obtained by interpolating the respective poloidal flux distribution on the tokamak grid points on the 2-D divertor contour, as used also in local expansion method. Figure 6(a) shows a small variation in the RMSD of ψ_{div} between EFITRT1 vs. local expansion (both relative to EFIT01), thereby demonstrating a similar performance with respect to the estimation of ψ_{div} . As would be expected based on the agreement in ψ_{div} values, EFITRT1 and local expansion agree well on R_{OSP} as well (Figure 6(b,c)). The relatively small difference in the RMSD (≈ 0.005 m) in R_{OSP} between EFITRT1 and EFIT01, Vs. the local flux expansion method and EFIT01 (Figure 5(b) and 6(c)), indicate that local flux expansion can work as well as EFITRT1 in determining the outer strike point radial location with a RMSD in R_{OSP} of less than ≈ 1 cm with respect to EFIT01. For a device

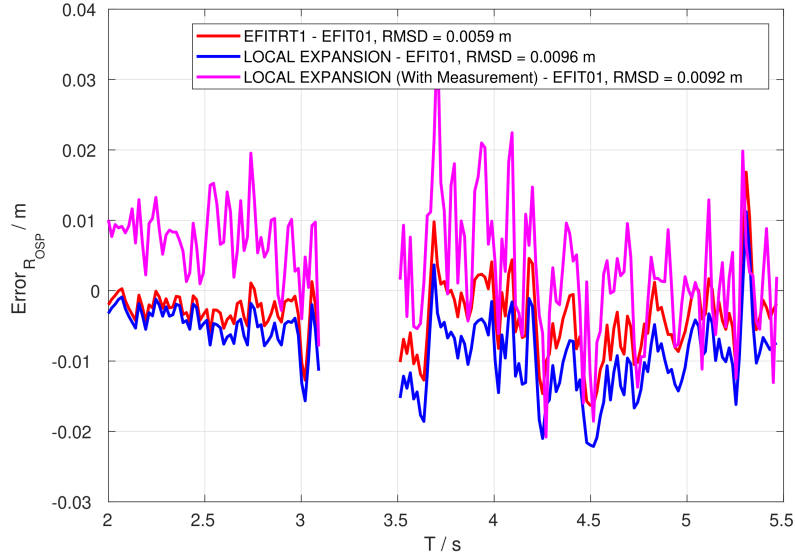


Figure 8: Effect of sensor measurements on the evolution of the error in R_{OSP} between the local expansion method with 6th order polynomial and EFIT01. The empty region between the time interval 3.1 s - 3.5 s denotes the transition of the plasma equilibrium from the floor to the divertor shelf and is not accounted for the analysis.

of DIII-D size, typical accuracy requirement for radial location of the strike point and most shape quantities is less than ≈ 1 cm and is typically $\approx 1-2$ % of the minor radius of a tokamak.

Figure 7 compares the poloidal flux map, along with the separatrix in the divertor region, between the local expansion method with 6th order polynomial Vs. EFITRT1 for the plasma discharge shown in Figure 2(a) at $T = 5$ s. A good agreement between the isoflux contours, along with the separatrix is observed, near the floor and shelf region of the divertor between local expansion and EFITRT1. However, small discrepancies between the isoflux contours are observed far from the divertor contour.

All the analysis shown so far, uses the estimated values of sensor data derived from the poloidal flux distribution of EFITRT1. This choice is made for the sake of determining the accuracy involved inherently in the local expansion method itself with respect to EFITRT1. Figure 8 shows the response on the error in R_{OSP} between EFITRT1 and the local expansion method by the using direct magnetic measurement for the sensor as inputs. The noise in the magnetic sensors results in a similar RMSD value of ≈ 0.009 m but has a maximum error in R_{OSP} of 0.0380 m (Figure 8). In comparison, a maximum error in R_{OSP} of 0.0150 m (Figure 8) is obtained for the case using the estimated sensor data from EFITRT1. Thus, the noise in the measurements play a key role with respect to the accuracy of the local expansion method and imposes a strong requirement on the signal to

noise ratio for the magnetic sensors.

5 Summary and outlook

Local expansion method developed for MAST-U for strike point position estimation was successfully implemented and benchmarked for a long legged DIII-D divertor plasma discharge. A good comparison of the outer strike position from EFIT01 and the Langmuir probe diagnostic data was observed, justifying the use of EFIT01 as the reference for comparing the performance of the local expansion method and EFITRT1. For the long legged divertor plasma with strike point sweeping, a 6th order polynomial expansion gave a good performance with the RMSD ≈ 0.005 m between the error in R_{OSP} between EFITRT1 and EFIT01, and the error in the local expansion method and EFIT01. The application using a DIII-D divertor plasma discharge indicated that local flux expansion can work as well as EFITRT1, in determining strike point locations. The difference in the RMSD between the error in R_{OSP} between 6th order local expansion method and EFIT01 Vs. EFITRT1 and EFIT01 was found to be ≈ 0.005 m. The RMSD of the error in R_{OSP} between 6th order local expansion method and EFIT01 was less than ≈ 1 cm, and satisfied the typical accuracy criteria of less than $\approx 1-2$ % of the minor radius for shape quantities, including strike point position for DIII-D. The effect of the noise in the sensor measurement on the local expansion method was studied and was found to play a key role in the successful application of the method for strike point position estimation. Sensor noise resulted in a similar RMSD value of 0.009 m between local expansion method and EFIT01. However, a maximum error in R_{OSP} of 0.0380 m compared to a maximum error of 0.0150 m for the case using the estimated sensor data from EFITRT1 was observed. However, the crucial result here is the internal consistency of the local expansion method, i.e. its ability to match the EFITRT1 accuracy for the case when sensor data is estimated from the poloidal flux distribution from EFITRT1. In other words, performance of the local expansion method with magnetic sensors with good signal to noise ratio would be able to match the accuracy levels sufficient for implementation on a tokamak.

Local expansion is fast to calculate and already implemented (as LEMUR: Local Expansion Mast Upgrade Reconstruction [19]) in MAST-U. The experimental validation of LEMUR with the RT equilibrium reconstruction is planned during the 2022 MAST-U campaign. Nevertheless, the results included in the paper are encouraging that the local expansion method can provide good accuracy in real-time, so detachment control systems for MAST-U can be designed with this in mind.

Acknowledgement and Disclaimer

Acknowledgement:

This material is based upon work supported by the U.S. Department of En-

ergy, Office of Science, Office of Fusion Energy Sciences, under Award(s) DE-SC0018992.

This work has been partly funded by EPSRC Grant is EP/T012250/1

Disclaimer: This report was prepared as an account of work sponsored by an agency of the United States Government. Neither the United States Government nor any agency thereof, nor any of their employees, makes any warranty, express or implied, or assumes any legal liability or responsibility for the accuracy, completeness, or usefulness of any information, apparatus, product, or process disclosed, or represents that its use would not infringe privately owned rights. Reference herein to any specific commercial product, process, or service by trade name, trademark, manufacturer, or otherwise does not necessarily constitute or imply its endorsement, recommendation, or favoring by the United States Government or any agency thereof. The views and opinions of authors expressed herein do not necessarily state or reflect those of the United States Government or any agency thereof.

6 Appendix

According to Equation 1, Equation 2 can be written as follows:

$$\sum_{\substack{i=1 \\ j=0}}^{i+j \leq n-1} 4i(i+1)a_{i+1,j}\rho^i z^j + \sum_{\substack{i=0 \\ j=0}}^{i+j \leq n-2} 4R_0^2(i+1)(i+2)a_{i+2,j}\rho^i z^j + \sum_{\substack{i=0 \\ j=0}}^{i+j \leq n-2} (j+1)(j+2)a_{i,j+2}\rho^i z^j \quad (7)$$

To satisfy Equation 7 at each point in the vacuum region, we force the coefficient of $\rho^i z^j$ to be zero. As a result, the number of coefficients in Equation 1 reduces.

For $n=4$, the number of independent coefficients is 6 and the poloidal flux expansion is as follow:

$$\psi = a_{00} + a_{01}z + a_{10}\rho + a_{11}\rho z + a_{20}(\rho^2 - 4R_0^2 z^2 - 4\rho z^2) + a_{21}(\rho^2 z - \frac{4}{3}R_0^2 z^3 - \frac{4}{3}\rho z^3) \quad (8)$$

For $n=5$, the number of independent coefficients is 7 and the poloidal flux expansion is as follow:

$$\psi = a_{00} + a_{01}z + a_{10}\rho + a_{11}\rho z + a_{20}(\rho^2 - 4R_0^2 z^2 - 4\rho z^2) + a_{21}(\rho^2 z - \frac{4}{3}R_0^2 z^3 - \frac{4}{3}\rho z^3) + a_{22}(\rho^2 z^2 - \frac{2}{3}R_0^2 z^4 - \frac{2}{3}\rho z^4 - \frac{1}{12}\rho^3 + R_0^2 \rho z^2) \quad (9)$$

For $n=6$, the number of independent coefficients is 8 and the poloidal flux expansion is as follow:

$$\begin{aligned}
\psi = & a_{00} + a_{01}z + a_{10}\rho + a_{11}\rho z + a_{20}(\rho^2 - 4R_0^2z^2 - 4\rho z^2) \\
& + a_{21}(\rho^2z - \frac{4}{3}R_0^2z^3 - \frac{4}{3}\rho z^3) + a_{22}(\rho^2z^2 - \frac{2}{3}R_0^2z^4 - \frac{2}{3}\rho z^4 - \frac{1}{12}\rho^3 + R_0^2\rho z^2) + \\
& a_{23}(\rho^2z^3 - \frac{2}{5}R_0^2z^5 - \frac{2}{5}\rho z^5 - \frac{1}{4}\rho^3z + R_0^2\rho z^3)
\end{aligned} \tag{10}$$

For $n=7$, the number of independent coefficients is 9 and the poloidal flux expansion is as follow:

$$\begin{aligned}
\psi = & a_{00} + a_{01}z + a_{10}\rho + a_{11}\rho z + a_{20}(\rho^2 - 4R_0^2z^2 - 4\rho z^2) \\
& + a_{21}(\rho^2z - \frac{4}{3}R_0^2z^3 - \frac{4}{3}\rho z^3) + a_{22}(\rho^2z^2 - \frac{2}{3}R_0^2z^4 - \frac{2}{3}\rho z^4 - \frac{1}{12}\rho^3 + R_0^2\rho z^2) + \\
& a_{23}(\rho^2z^3 - \frac{2}{5}R_0^2z^5 - \frac{2}{5}\rho z^5 - \frac{1}{4}\rho^3z + R_0^2\rho z^3) + \\
& a_{24}(\rho^2z^4 - \frac{4}{15}R_0^2z^6 - \frac{4}{15}\rho z^6 - \frac{1}{2}\rho^3z^2 + \frac{1}{2}R_0^4\rho z^2 + R_0^2\rho z^4 - \frac{1}{24}R_0^2\rho^3 - \frac{1}{48}\rho^4)
\end{aligned} \tag{11}$$

References

- [1] G. Fishpool, J. Canik, G. Cunningham, J. Harrison, I. Katramados, A. Kirk, M. Kovari, H. Meyer, and R. Scannell, “MAST-upgrade divertor facility and assessing performance of long-legged divertors”, *Journal of Nuclear Materials* **438**, S356 (2013), ISSN 00223115, doi:10.1016/j.jnucmat.2013.01.067.
- [2] P. M. Valanju, M. Kotschenreuther, S. M. Mahajan, and J. Canik, “Super-X divertors and high power density fusion devices”, *Physics of Plasmas* **16** (2009), ISSN 1070664X, doi:10.1063/1.3110984.
- [3] C. Guillemaut, M. Lennholm, J. Harrison, I. Carvalho, D. Valcarcel, R. Felton, S. Griph, C. Hogben, R. Lucock, G. F. Matthews, C. P. V. Thun, R. A. Pitts, S. Wiesen, and JET contributors, “Real-time control of divertor detachment in h-mode with impurity seeding using langmuir probe feedback in JET-ITER-like wall”, *Plasma Phys. Control. Fusion* **59**, 045001 (2017), doi:10.1088/1361-6587/aa5951.
- [4] J. R. Ferron, M. L. Walker, L. L. Lao, H. E. John, D. A. Humphreys, and J. A. Leuer, “Real time equilibrium reconstruction for tokamak discharge control”, *Nuclear Fusion* **38**, 1055 (1998), ISSN 0029-5515, doi:10.1088/0029-5515/38/7/308.
- [5] J. M. Moret, B. P. Duval, H. B. Le, S. Coda, F. Felici, and H. Reimerdes, “Tokamak equilibrium reconstruction code LIUQE and its real time implementation”, *Fusion Engineering and Design* **91**, 1 (2015), ISSN 09203796, doi:10.1016/j.fusengdes.2014.09.019.
- [6] D. A. Gates, J. R. Ferron, M. Bell, T. Gibney, R. Johnson, R. J. Marsala, D. Mastrovito, J. E. Menard, D. Mueller, B. Penafior, S. A. Sabbagh, and T. Stevenson, “Plasma shape control on the National Spherical Torus Experiment (NSTX) using real-time equilibrium reconstruction”, *Nuclear Fusion* **46**, 17 (2005), ISSN 0029-5515, doi:10.1088/0029-5515/46/1/002.
- [7] J. Milnes, N. B. Ayed, F. Dhalla, G. Fishpool, J. Hill, I. Katramados, R. Martin, G. Naylor, T. O’Gorman, and R. Scannell, “MAST upgrade - Construction status”, *Fusion Engineering and Design* **96-97**, 42 (2015), ISSN 09203796, doi:10.1016/j.fusengdes.2015.03.002.
- [8] D. P. O’Brien, J. J. Ellis, and J. Lingertat, “Local expansion method for fast plasma boundary identification in JET”, *Nuclear Fusion* **33**, 467 (1993), ISSN 00295515, doi:10.1088/0029-5515/33/3/I08.
- [9] Y. Guo, B. Xiao, and Z. Luo, “A local expansion method applied to fast plasma boundary reconstruction for EAST”, *Plasma Physics and Controlled Fusion* **53** (2011), ISSN 07413335, doi:10.1088/0741-3335/53/10/105015.

- [10] J. L. Luxon, “A design retrospective of the DIII-D tokamak”, *Nuclear Fusion* **42**, 614 (2002), ISSN 00295515, doi:10.1088/0029-5515/42/5/313.
- [11] E. J. Strait, “Magnetic diagnostic system of the DIII-D tokamak”, *Review of Scientific Instruments* **77** (2006), ISSN 00346748, doi:10.1063/1.2166493.
- [12] L. L. Lao, H. E. St John, Q. Peng, J. R. Ferron, E. J. Strait, T. S. Taylor, W. H. Meyer, C. Zhang, and K. I. You, “MHD equilibrium reconstruction in the DIII-D tokamak”, *Fusion Science and Technology* **48**, 968 (2005), ISSN 15361055, doi:10.13182/FST48-968.
- [13] L. L. Lao, H. St. John, R. D. Stambaugh, A. G. Kellman, and W. Pfeiffer, “Reconstruction of current profile parameters and plasma shapes in tokamaks”, *Nuclear Fusion* **25**, 1611 (1985), ISSN 0029-5515, doi:10.1088/0029-5515/25/11/007.
- [14] T. Eich, B. Sieglin, A. Scarabosio, W. Fundamenski, R. Goldston, A. Herrmann, and ASDEX Upgrade Team, “Inter-ELM power decay length for JET and ASDEX upgrade: Measurement and comparison with heuristic drift-based model”, *Phys. Rev. Lett.* **107**, 215001 (2011), doi:10.1103/PhysRevLett.107.215001.
- [15] J. G. Watkins, D. Taussig, R. L. Boivin, M. A. Mahdavi, and R. E. Nygren, “High heat flux langmuir probe array for the DIII-D divertor plates”, *Rev. Sci. Instrum.* **79**, 10F125 (2008), doi:10.1063/1.2982423.
- [16] L. Tonks and I. Langmuir, “A general theory of the plasma of an arc”, *Phys. Rev.* **34**, 876 (1929), doi:10.1103/PhysRev.34.876.
- [17] T. D. Rognlien, D. D. Ryutov, N. Mattor, and G. D. Porter, “Two-dimensional electric fields and drifts near the magnetic separatrix in divertor tokamaks”, *Phys. Plasmas* **6**, 1851 (1999), doi:10.1063/1.873488.
- [18] D. Eldon, A. Hyatt, B. Covele, N. Eidietis, H. Guo, D. Humphreys, A. Moser, B. Sammulu, and M. Walker, “High precision strike point control to support experiments in the DIII-D small angle slot divertor”, *Fusion Engineering and Design* **160**, 111797 (2020), doi:https://doi.org/10.1016/j.fusengdes.2020.111797.
- [19] G. McArdle, L. Pangione, and M. Kochan, “The MAST Upgrade plasma control system”, *Fusion Engineering and Design* **159**, 111764 (2020), ISSN 0920-3796, doi:https://doi.org/10.1016/j.fusengdes.2020.111764.